Mixing and segregation of microspheres in microchannel flows of mono- and bidispersed suspensions

C. Gao, B. Xu, and J. F. Gilchrist*
Department of Chemical Engineering, Lehigh University, Bethlehem, Pennsylvania 18015, USA
(Received 16 October 2008; published 20 March 2009)

We investigate the mixing and segregation of mono- and bidispersed microsphere suspensions in microchannel flows. These flows are common in biological microelectromechanical systems (BioMEMS) applications handling blood or suspensions of DNA. Suspension transport in pressure driven flows is significantly hindered by shear-induced migration, where particles migrate away from the walls and are focused in the center due to multibody hydrodynamic interactions. The microchannels used in this study have geometries that induce chaotic advection in Newtonian fluids. Our results show that mixing in straight, herringbone and staggered herringbone channels depends strongly on volume fraction. Due to this complex interplay of advection and shear-induced migration, a staggered herringbone channel that typically results in chaotic mixing is not always effective for dispersing particles. The maximum degree of segregation is observed in a straight channel once the maximum packing fraction is reached at channel center. We modify a one-dimensional suspension balance model [R. Miller and J. Morris, J. Non-Newtonian Fluid Mech. **135**, 149 (2006)] to describe the behavior at the center of the straight channel. The degree of mixing is then calculated as a function of bulk volume fraction, predicting the volume fraction that results in the maximum degree of segregation. In bidispersed suspension flow, it is shown that mixing of the larger species is enhanced in straight and staggered herringbone channels while segregation is enhanced at moderate volume fractions in herringbone channels. This suggests mixing and separations can be tailored by adjusting both the suspension properties and the channel geometry.

DOI: 10.1103/PhysRevE.79.036311 PACS number(s): 47.57.−s, 47.52.+j, 47.61.Ne

I. INTRODUCTION

Mixing of Newtonian fluids at small scales is well known to be difficult due to small Reynolds numbers, often high Péclet numbers, and difficulty in applying conventional approaches used at the macroscale. To enhance mixing, it has been shown that chaotic flows can be generated either by changing geometry [1], such as serpentine [2], zigzag channels [3], split-and-recombine channels [4], or by modulating the external energy, including periodic flow switching, fluctuating electrical fields, and ultrasound [5]. Stroock *et al.* [6] introduced the staggered herringbone geometry to enhance mixing successfully at the microscale without significantly increasing the resistance to the flow, common in baffled flows. Circulation generated in the transverse direction to the main axis of flow enhances near-wall transport. By breaking left-right symmetry periodically along the axis of flow, the fluid experiences an effective blinking vortex that breaks streamlines to induce chaotic advection.

The behavior of suspensions, however, is much more complicated. It is often assumed in device design that particles will simply follow the streamlines of the underlying flow, commonly used in velocimetry. However, at moderate concentrations, particle-wall and particle-particle interactions can generate irreversible migration across streamlines. The result can lead to the generation of relatively strong concentration gradients in the flow field, effectively demixing the suspension. It is the particle collisions which are generally associated with diffusion of particles that generate the normal stresses which cause heterogeneity in the concentration profiles. This so-called shear-induced migration [7], studied primarily in simple one-dimensional (1D) shear flows, is highly complicated and generates interplay with the underlying flow because of the local variations in viscosity due to migration. In a pressure driven flow between two parallel walls, particles migrate toward the central region of lower shear and flatten the velocity profile because of the gradient of concentration-dependent viscosity. This interplay has been recently explored in more complicated microchannel flows intended to enhance transport both experimentally [8] and numerically [9].

Suspensions of particles with polydispersed physical and chemical properties are common in natural processes such as blood flow and sediment transport in rivers, bioengineering analyses of cellular and DNA material, and industries including coatings, coal, food, and pharmaceuticals. The properties of the suspension have a large effect on the details of mixing and segregation. It is well known that the addition of smaller particles into a monodispersed suspension can increase the possible maximum packing fraction of the particle phase [10,11] and lower the relative viscosity of the suspension [12,13], however fewer studies have focused on the rheology of bidispersed suspensions of particles varying in size. Seminal work includes studies of suspensions having equal volume fractions of large and small particles, studied by Lyon and Leal [14] between parallel walls. They found that away from channel walls each of the large and small particle species will have similar concentration profiles at $\phi_{\text{bulk}}=0.4$. Shauly *et al.* [15] showed by simulation of flow in a Couette device that the addition of small particles leads to stronger migration for large particles, and higher concentration of small particles are found in high-shear areas. Semwogerere and Weeks [16] showed that between parallel walls the concentration profile of large particles is mostly independent of the addition of small particles. Norman *et al.* [17] demon-

*gilchrist@lehigh.edu

strated that in pipe flows the addition of large and neutrally buoyant particles helps to resuspend heavier small particles. All of these studies focus on steady 1D flows that have closed streamlines, and this cross section of the literature suggests the behavior of bidispersed suspensions in simple flows is complex.

The primary questions investigated in this paper are, how will transverse flow circulation and the addition of smaller particles affect the mixing of particles inside main channels? and what is the best way to mix concentrated particle suspension in microchannels? To address these questions, we studied the 1D, two-dimensional (2D), and three-dimensional (3D) chaotic flows of mono- and bidispersed suspensions of microspheres from dilute to moderate concentrations which can result in the formation of regions of high concentration.

II. EXPERIMENTAL

A. Materials

The monodispersed suspension consists of $2a=1.01\pm0.02$ μm (a, particle radius) monosized silica microspheres ($\rho=2.0$ g/cm^3, Fuso Chemical Co.) at volume fractions $0.02\leq\phi_{\text{bulk}}\leq0.3$ in a 3:1 (by volume) glycerin:water mixture ($\eta_0=0.04$ Pa s, $\rho=1.20$ g/cm^3) to refractive index match the microspheres. The bidispersed suspension consists of larger particles ($2a=1.01\pm0.02$ μm) and smaller particles ($2a=0.51\pm0.02$ μm) with equal volume fractions and total volume fractions of 0.04, 0.1, 0.2, and 0.3. The solution is adjusted to pH=8.0 and 0.025 mM $NaNO_3$ to produce a Debye screening length $\kappa^{-1}=1.5$ nm on the charge-stabilized microspheres and 0.1 mM Rhodamine B is added as fluorescence for imaging. Flow is driven by a syringe pump (Harvard Apparatus) resulting in a maximum velocity of 200 μm/s, as determined by velocimetry, at Pe $=5100$ ($\text{Pe}\equiv\frac{6\pi\eta_0\dot{\gamma}a^3}{kT}$ for shear rate $\dot{\gamma}=\frac{v_{\max}}{H}$, where H is the half-height of the channel, k is the Boltzmann constant, and T is the absolute temperature) and $\text{Re}=8.2\times10^{-7}$ ($\text{Re}\equiv\frac{\rho a^2\dot{\gamma}}{\eta_0}$). Final patterns in these geometries have been studied up to $\text{Pe}=1.2\times10^5$ ($\text{Re}=2\times10^{-5}$) and are general at the high Pe and low Re limit.

B. Flow device

Microchannels are fabricated via soft lithography [18] using silicon wafer masks fabricated at Cornell NanoScale Facility to construct two-level etched structures (for both the main channel and the herringbones) to be imprinted into polydimethylsiloxane [(PDMS), Dow Corning]. First, channel structures are etched onto a silicon wafer. Next, two plastic connectors (Harvard Apparatus) are placed on top of the wafer and filled with water to inhibit infiltration of PDMS into the primary flow path. Elastomer base mixed with curing agent is gently poured onto the wafer, surrounding the connectors and the etched channels. After being heated for 30 min at 80 °C, the PDMS cures, then the pattern and embedded connectors can be lifted from the wafer. After treating both this structure and a glass coverslip in a plasma cleaner (Harrick Plasma) for 2 min, the PDMS readily bonds with the glass and the channel is contained within. The bond is sufficiently strong to withstand relatively high pressures necessary to produce moderate flow rates within the channel. One inlet is connected to a syringe powered by a syringe pump (Harvard Apparatus) and the other connector acts as a reservoir (Fig. 1). The main channel flow path is width $\times$ depth $\times$ length $=100$ μm $\times 40$ μm $\times 30$ mm. A straight channel (STR) generates 1D flows, a herringbone (HB) channel generate 2D flows with symmetric flow circulations across the main channel (flow penetrating down near the top of the channel and outward toward the walls near the bottom), and a staggered herringbone (SHB) channel produces 3D chaotic flows with axially alternating asymmetric flow circulations across the main channel (Fig. 1). To ensure that the final concentration patterns are fully developed, measurements are taken far from the entrance when the suspension stresses are balanced again, $\frac{L}{H}>2000$ where L is the length of the channel, for these conditions [19]. Convergence is validated periodically by scanning at a location closer to the entrance and comparing results.

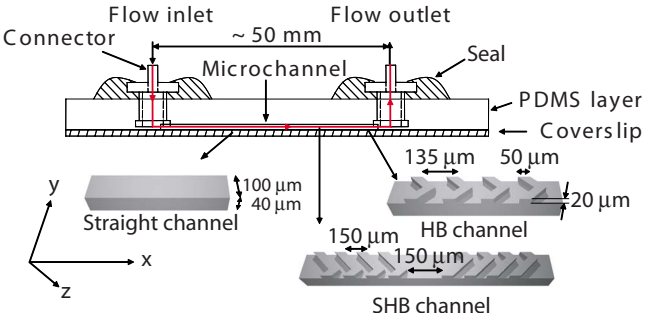

FIG. 1. (Color online) Schematic of the flow device and microchannel geometries. Microchannels are either straight, HB, or SHB channels having 45° baffles along the top of the channel. The red line with arrows shows the flow path.

C. Imaging and data analysis

Confocal laser scanning microscopy [(CLSM), VTeye, VisiTech International] is used to study the suspension flow in each microchannel. The advantages of CLSM—fast scanning (up to 400 fps), a thin sampling region (~0.5 μm), and fast rastering of confocal plane (~170 steps/s)—enable 3D z-stack scanning (Fig. 2) to track particles through the depth of the microchannel. Concentration profiles are generated from six columns of overlapping image stacks covering the

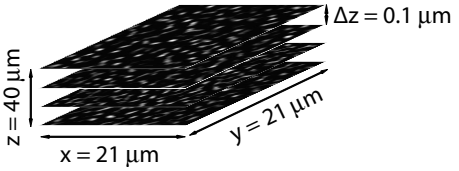

FIG. 2. 3D z-stack image scanning. One single confocal image (21×21 μm^2) is captured every 100 nm in the z direction, bandpass images are shown here with bright spots representing particles. The confocal plane scans across the full depth of the 40 μm channel.

whole width of the main channel, each representing $21 \times 21 \times 40$ μm^3. Data are averaged in the x direction (~ 20 μm) and over nine z-stack scans, each taken at 170 fps to reduce distortions related to velocity in the z direction in 2D and 3D flows. At each location, the standard error is less than 1% of the reported value. The locations of particles, determined by using code developed by Eric Weeks at Emory University using algorithms developed by Crocker and Grier [20], are binned by 1×1 μm^2 to represent local concentrations and then normalized to verify ϕ_{bulk}. Selected experiments were stopped and scanned to assure the value of ϕ_{bulk} matched that of the prepared suspension. These values match due to a 15° converging entrance that also mitigates near-wall migration upstream. Regions neighboring the channel walls have been clipped uniformly to avoid inaccuracy in particle tracking.

III. RESULTS

A. Monodispersed suspension

Figure 3 shows the quantitative transverse concentration profiles in 1D, 2D, and 3D flows. For all channels at low bulk volume fraction $\phi_{bulk}=0.02$ gradients due to density mismatch between fluids and particles are apparent ($\Delta\rho = 0.8$ g/cm^3), and as expected from previous results [21] no evidence of shear migration is present. At $\phi_{bulk}=0.05$, both the straight and SHB channels also only display gravity-driven gradients. The 2D flow in the HB channel demonstrates an emergence of a vertically oriented low-concentration band in the center of the channel. The two regions of significantly higher ϕ suggest the concentration gradients are a result of the onset of shear-induced migration. This demonstrates that the onset of shear migration occurs $0.05 < \phi_{bulk} < 0.10$. In previous work [22], the threshold for shear-induced migration is roughly $\phi_{bulk}=0.2$ for particles $2a=650$ μm, a discrepancy that could be related to the small amount of electrostatic interactions in this charge-stabilized suspension or a result of confinement in both y and z. At $\phi_{bulk}=0.10$, the effect of shear migration is clear in 1D, 2D, and 3D flows, however mixing in the 3D flow partially inhibits localized coarsening of particle volume fraction.

At higher concentrations, the effects of gravity appear to be completely mediated, especially in 1D and 2D flows. Strong concentration gradients are apparent for $\phi_{bulk} \geq 0.20$. All 1D flows show essentially the same pattern for different concentrations, highest at the center and decreasing steadily toward the channel walls. Similarly, the 2D profile exhibits two regions of higher concentration that correspond roughly to the streamlines in the transverse direction, however the concentration in the center increases dramatically and is not nearly as depleted of particles as at lower concentrations near $\phi_{bulk}=0.10$. In the 3D flow, which for Newtonian systems mix the best, high-concentration gradients exist, driving particles near the lower boundary. This is not a result of gravity, and is more likely related to the lower degree of transverse shear located away from the herringbones at the lower wall.

Intensity of segregation, used as a tool to compare these results across the various flow profiles, is defined as

$$I \equiv \frac{\sigma^2}{\phi_{bulk}(\phi_{max} - \phi_{bulk})} \quad (1)$$

based on the definition given by Danckwerts [23], where σ is the standard deviation of local concentrations and $\phi_{max}=0.62$ is taken as the maximum packing fraction for randomly packed hard spheres. $I=0$ indicates perfect mixing and $I=1$ occurs for perfect segregation. It is known that higher ϕ_{bulk} generates a stronger driving force for shear-induced migration [7,19,24]. However the influence of this segregation is mediated by collisional diffusivity and volume exclusion at the highest ϕ_{bulk}. Of course, at both $\phi_{bulk}=0$ and $\phi_{bulk}=\phi_{max}$ there is no net migration. Therefore, at an intermediate ϕ_{bulk}, the resulting concentration gradients in the channel should result in a maximum in I.

Figure 4 shows the intensity of segregation of particles in monodispersed suspension for the 1D, 2D, and 3D flows with $0.02 \leq \phi_{bulk} \leq 0.3$. Those values for experiments $\phi_{bulk} < 0.2$ are likely larger than expected from shear-induced migration alone due to the buoyancy-driven drift. The error in the reported data is less than 1% of each reported value, and consistency between experiments is relatively high, depending primarily on the reproducibility of the channel fabrication. At $\phi_{bulk}=0.15$, the 1D flow apparently demonstrates less shear-driven segregation than either the HB or the SHB channels. At $\phi_{bulk}=0.2$, the 2D flow interplays with the flow such that the overall intensity of segregation is highest, and at $\phi_{bulk}=0.25$ this straight channel displays the strongest segregation. As is seen in Fig. 3 for 1D experiments at these higher ϕ_{bulk}, we observe a thin horizontal region of roughly two to three particle diameters wide of highly packed particles ($\phi \sim 0.50$) in straight channel center after $\phi_{bulk} \geq 0.24$. The maximum concentration is constant and width of this region in the y direction increases as ϕ_{bulk} increases. Note that the shear gradient is stronger in the z direction, but the overall profile is influenced by the shear in the y direction. This suggests that in these experiments of charge-stabilized spheres, ϕ_{max} is perhaps lower than the maximum packing fraction for hard spheres. Likewise, it is unlikely that thermal rearrangements that cause higher ordering occur in the short-time scale of this experiment. While it is reasonable to expect only one maximum in the intensity of segregation as a function of ϕ_{bulk} in the 1D flow, it is unclear from this data whether another local maximum may occur at higher values of ϕ_{bulk} or between data points sampled here. This is especially true for the 3D flow, where often chaotic advection causes a high degree of parametric sensitivity.

B. Modeling and analysis

In an attempt to compare the results found in this study to existing theory, and to offer a theoretical basis for predicting the maximum in the intensity of segregation profile, a suspension stress model is used to fit the data and extrapolate beyond the parameters tested experimentally. We only analyze the data from the center of the straight channels investigating the shear in the z direction, which is much stronger than the shear in the y direction; studies modeling 2D and 3D chaotic flows that demonstrate coarsening via shear-induced

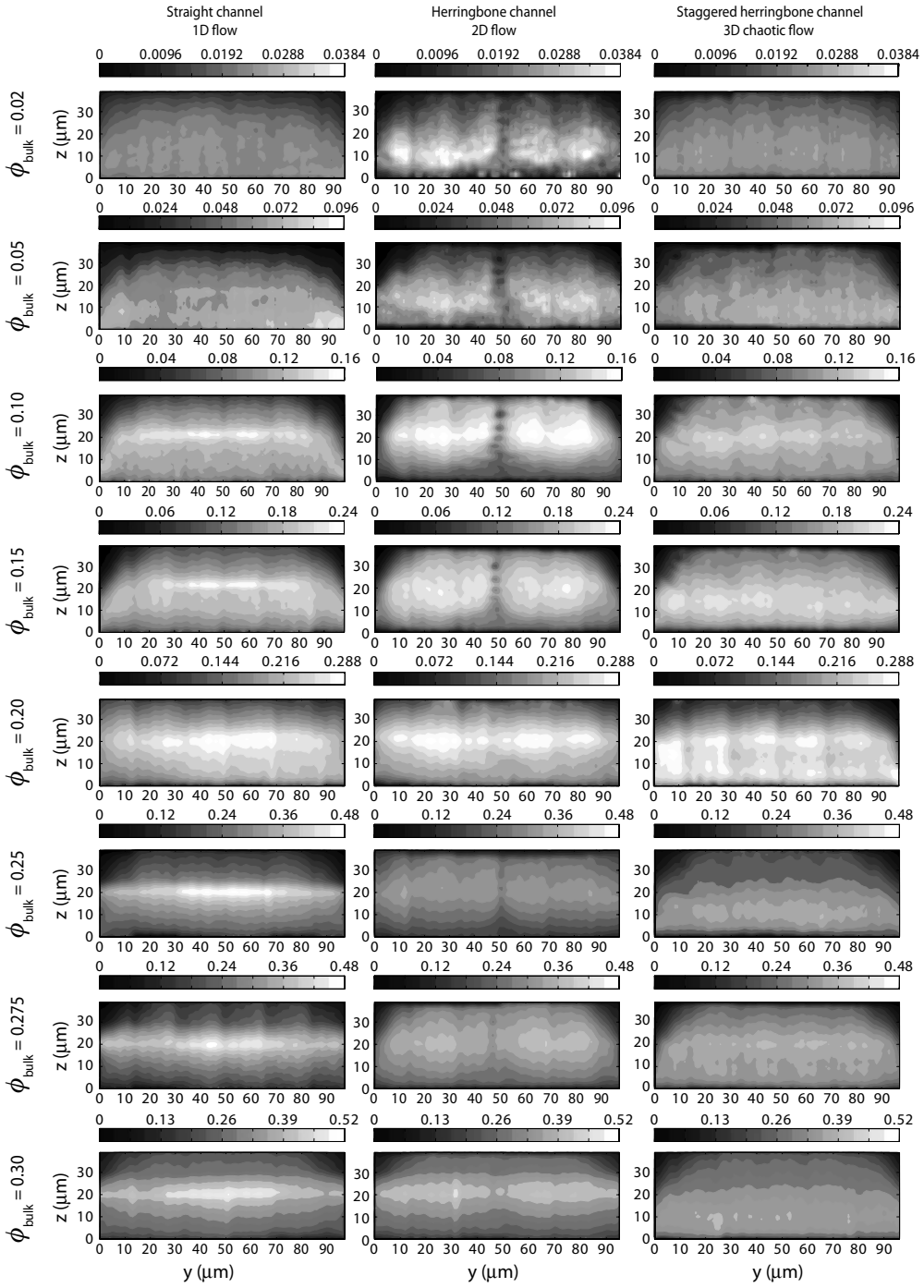

FIG. 3. Spatial concentration profiles of ϕ in the transverse direction to the pressure-driven flow for $0.02 \leq \phi_{\text{bulk}} \leq 0.3$ in 1D, 2D, and 3D flows of the monodispersed suspensions.

migration are ongoing. The model follows closely the work by Miller and Morris [25] to analyze the data from the center of the 1D flow. In a fully developed pressure-driven 1D suspension flow at steady state, the normal stress in the particulate phase must balance,

$$\nabla \cdot \Sigma_P^{\text{NS}} = \frac{\partial \Sigma_{P,zz}^{\text{NS}}}{\partial z} = 0 \tag{2}$$

where Σ_P^{NS} is the normal stress tensor in particulate phase, and z is the direction of velocity gradient. Because of the aspect ratio of the 1D channel used in this study, the migration at the center of the channel is strongly dependent on the shear in z direction, while the configuration in y direction is relatively uniform. Thus, only data within ± 20 μm from the center in the y direction are evaluated without consideration of the sidewalls.

It should also be noted that when considering the data at the center of the channel, the apparent bulk volume fraction (ϕ_{bulk}^a) in this region is significantly higher due to particle depletion near the side walls. Likewise, only data free of the

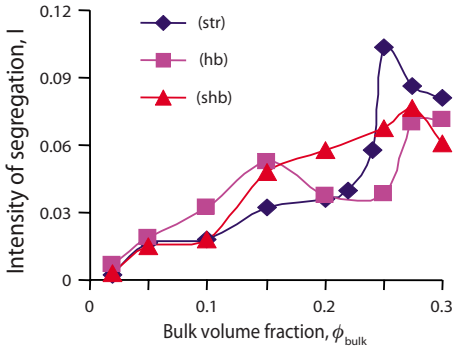

FIG. 4. (Color online) The intensity of segregation for 1D (STR), 2D (HB), and 3D (SHB) flows of monodispersed suspensions at ϕ_{bulk} from 0.02 to 0.3.

gravitational effects, i.e., at higher values of ϕ_{bulk}, are evaluated. For the above-mentioned reasons, another set of experiments was carried out in the straight channels with smaller concentration intervals between 0.2 and 0.35: ϕ_{bulk}=0.21, 0.22, 0.24, 0.275, 0.3, 0.33, and 0.35, with their corresponding ϕ^a_{bulk}=0.25, 0.27, 0.29, 0.34, 0.37, 0.39, and 0.41.

Particle phase normal stress can be expressed as [25]

$$\Sigma_P^{NS} = -\eta_n(\dot{\gamma} + \dot{\gamma}_{NL})\mathbf{Q}, \tag{3}$$

where

$$\eta_n = \frac{0.75\eta_0(\phi/\phi_m)^2}{(1-\phi/\phi_m)^2} \tag{4}$$

is the estimation of the normal stress viscosity [26], $\dot{\gamma}$ is the local shear rate, and $\mathbf{Q}$ is a constant tensor describing the anisotropy of the flow. $\dot{\gamma}_{NL}$ is the nonlocal shear rate. Without $\dot{\gamma}_{NL}$, this model inaccurately predicts a physically unrealistic sharp peak in concentration at the center as a result of the local shear rate, $\dot{\gamma}$=0. The inclusion of $\dot{\gamma}_{NL}$ accounts for effects of finite particle size and higher order interactions that occur for moderate to high ϕ. In the previous work, they assume that $\dot{\gamma}_{NL}$ is primarily a function of particle size [25]. Other models also use various methods to resolve this singularity (e.g., [19,27,21]). The analysis presented here assumes that $\dot{\gamma}_{NL}$ is a function of ϕ_c, the local central volume fraction, which is also the maximum volume fraction measured in each profile. All concentrations are averaged over one-particle diameter to represent the effective averaging resulting from the experimental measurement. To simplify the analysis, the nonlocal shear rate is assumed to be constant across the channel. The value of $\dot{\gamma}_{NL}$ will only be significant near the center where $\dot{\gamma}$=0. Without a strong first-principles understanding of the origin of the nonlocal shear, $\dot{\gamma}_{NL}$ is used as a fitting parameter for the experimental data.

The resulting predicted profiles of volume fraction are plotted against the experimental data sampled near the channel center in Fig. 5. Data near the wall are excluded in the analysis. The migration near the wall is enhanced by particle-wall interactions which are excluded from this normal stress balance. The model fits the data well, based on an optimum value of $\dot{\gamma}_{NL}$. The empirical relation between $\dot{\gamma}_{NL}$ and ϕ_c

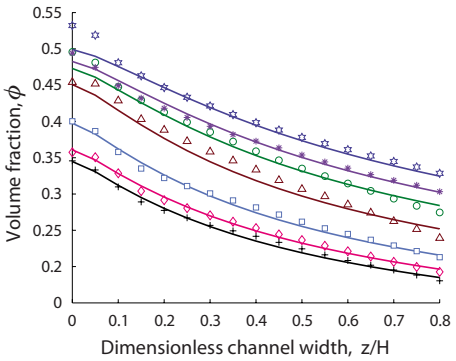

FIG. 5. (Color online) Model (solid lines) vs experiment at average volume fractions, ϕ^a_{bulk}=0.25 (crosses), 0.27 (diamonds), 0.29 (squares), 0.34 (triangles), 0.37 (circles), 0.39 (asterisks), and 0.41 (hexagrams).

near the center of the channel in the z-direction is shown in Fig. 6. The magnitude of $\dot{\gamma}_{NL}$ is typically 10% of the average local shear rate. A power-law fit results in

$$\dot{\gamma}_{NL} = 0.0176(\phi_c)^{-2.91}. \tag{5}$$

For unexplained reasons, this is approximately the inverse cube of the volume fraction, perhaps giving insight into the physical nature of $\dot{\gamma}_{NL}$ with relation to the transition from fluidlike to solidlike behavior of the normal stress. Indeed this relation does not apply to the low-concentration limit.

The fitting in Eq. (5) allows extension of the model to predict the volume fraction profile at different ϕ^a_{bulk} and thus the corresponding intensity of segregations. Figure 7 demonstrates the predicted intensity of segregation for different average volume fractions. It is clearly seen that the model captures the general trend of intensity of segregation. It is predicted that for a 1D system, i.e., pressure driven flow between parallel planes, shear-induced migration is strongest (poorest mixing) near ϕ^a_{bulk}=0.38. The experimental data also show a decrease in the intensity of segregation roughly for ϕ^a_{bulk}>0.34 (subject to noise), which supports the prediction from the model. Furthermore, the shear induced at the sidewalls causes demixing at significantly lower volume fractions. The effect of sidewalls and the channel aspect ratio

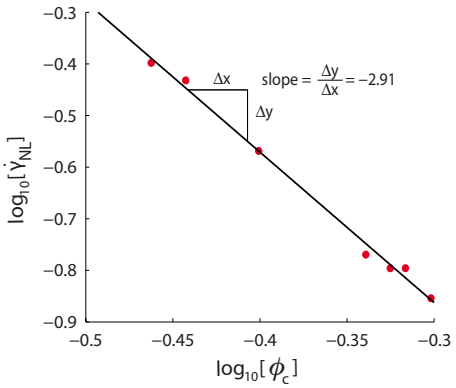

FIG. 6. (Color online) Power law correlation between the nonlocal shear rate $\dot{\gamma}_{NL}$ and volume fraction at channel center, ϕ_c.

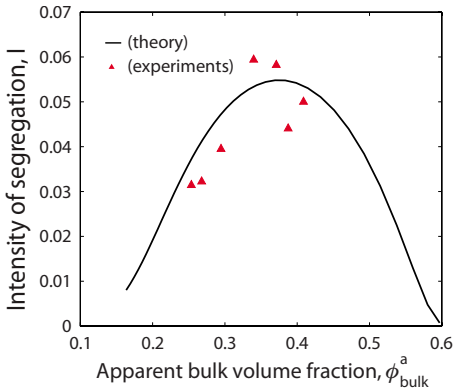

FIG. 7. (Color online) Predicted intensity of segregation vs experiment.

is a subject of ongoing study, having strong ramifications during device design at the microscale.

C. Bidispersed suspension

To study the effect of a smaller species on the migration of a suspension, 0.5 μm particles were added to the 1.0 μm monosized suspensions at $0.02 \leq \phi_{bulk} \leq 0.15$ at equal concentrations. Unfortunately, identification of the smaller species is inaccurate and thus not reported. Figure 8 shows the quantitative transverse concentration profiles of large particles in 1D, 2D, and 3D flows of bidispersed suspension with equal volume fractions of small particles at ϕ^L_{bulk} (large particles). At $\phi^L_{bulk}=0.02$ ($\phi_{bulk}=0.04$), the large particles are dispersed throughout the straight channel, a band of slightly lower concentration in HB channel exists, and a horizontal band of weakly higher concentration in SHB channels is visible. As in the monodispersed case, there is also evidence of gradients resulting from the density mismatch. At $\phi^L_{bulk}=0.05$, there is some evidence that a center band of higher concentration is forming in both the straight channel and SHB channel. Visual inspection of the frames captured verifies there are many more 0.5 μm particles near the bottom surface than the center or the top of the SHB channel. Because one would expect the larger particles to settle much faster, this suggests that the interplay between chaotic advection and migration is only weakly influenced by gravity. The HB channel has a clear central region that is depleted of larger particles, similar to that in the monosized suspension. For $\phi^L_{bulk}=0.1$, both the straight and SHB channel demonstrate clear effects of shear-induced migration, and the SHB profile differs from the monosized profile in that the highest concentration is located slightly above center, as opposed to near the bottom wall. The central band in the HB channel is not as clearly defined. Finally, at $\phi^L_{bulk}=0.15$, all of the profiles look similar to the monosized profiles.

Figure 9 shows the intensity of segregation based on measurements of ϕ^L_{bulk} (large particles) for 1D, 2D, and 3D flows of mono- and bidispersed suspensions with same volume fractions of small particles, respectively, with ϕ^L_{bulk} at 0.02, 0.05, 0.1, and 0.15 for bidispersed suspension flows. Once again, for $\phi_{bulk} \leq 0.15$, buoyancy plays a role in the segregation profiles. This should result in a higher than expected value for I, affecting the measurements of the monosized experiments more than the bidispersed suspension experiments. Thus, the intensity of segregations of bidispersed suspensions is generally higher than those in monodispersed suspensions at $0.02 \leq \phi^L_{bulk} \leq 0.15$. For $\phi_{bulk} \geq 0.2$, the straight and SHB channels continue to suggest that segrega-

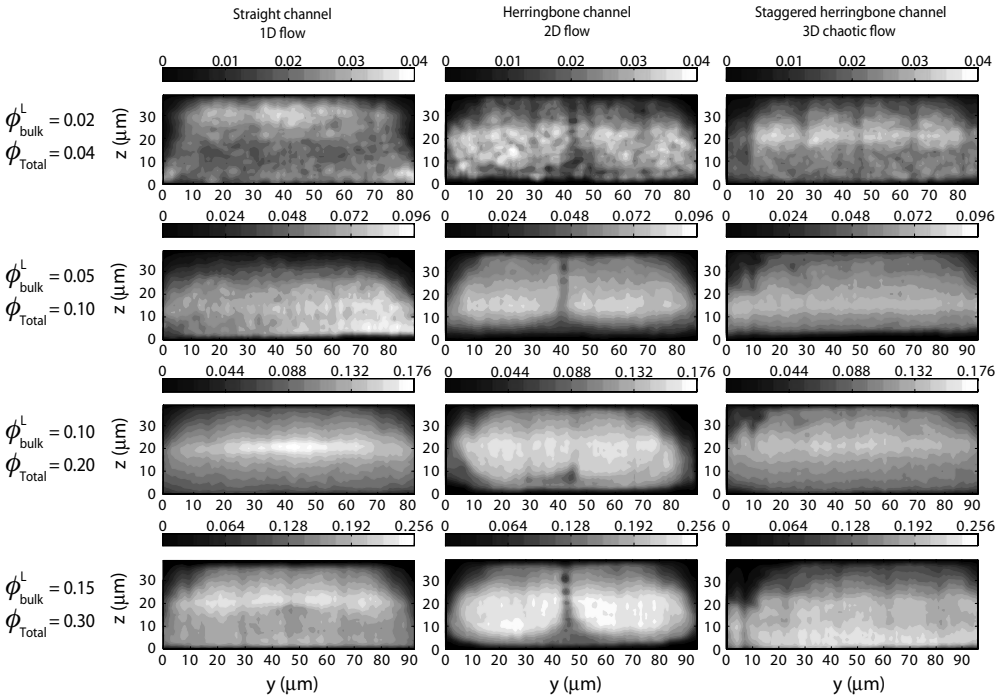

FIG. 8. The concentration profiles of large particles in the transverse direction to the pressure-driven in 1D, 2D, and 3D flows of bidispersed suspensions with equal volume fractions of small particles.

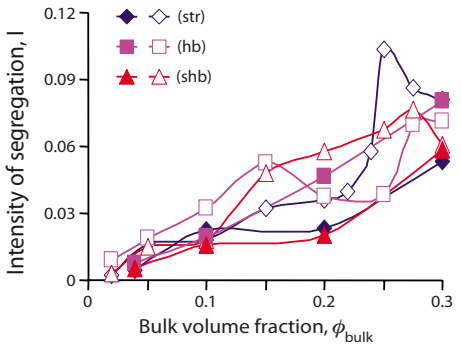

FIG. 9. (Color online) Comparison of the intensity of segregation for 1D (STR), 2D (HB), and 3D (SHB) flows of mono- and bidispersed suspensions with same volume fractions of small particles at ϕ^L_{bulk} (large particles) at 0.02, 0.05, 0.1, and 0.15. Empty symbols are for monodispersed suspensions and filled symbols are for large particles in bidispersed suspensions.

tion is inhibited when replacing half of the particles in solution with a smaller species. However, in HB channels the intensity of segregation for the bidispersed system is greater than that of the monodispersed suspension. This is a result of the larger particles preferentially moving toward the center of each of the two transverse recirculating regions. This demonstrates that the geometry can be modified to enhance or inhibit mixing selectively for bidispersed suspensions. Analogously, the suspension properties for a given channel can be altered to enhance or inhibit mixing.

IV. CONCLUSIONS

In summary, the behavior of particle suspensions in all three microchannel flows is much more complicated than that of Newtonian fluids. Shear-induced migration inhibits mixing while flow circulations in the main channel do not necessarily enhance mixing. By comparing these results to a normal stress balance model, the dependence of the nonlocal shear on volume fraction allows prediction of the theoretical maximum demixing that results from shear migration. In addition, it is found that polydispersity influences the mixing of large particles in bidispersed suspensions having the same volume fraction of small particles. The effect of polydispersity is also highly geometry dependent. Questions remain regarding how to design flows to effectively mix or segregate particles in microchannels, and the implications of this work will likely impact design of microscale mixers and separations used in handling suspensions, commonly found in BioMEMS applications designed to analyze blood or concentrated suspensions of DNA.

ACKNOWLEDGMENTS

The authors thank J. Morris and J. Brady for insightful conversations on suspension transport, E. Weeks for discussions regarding microfluidics and confocal microscopy, A. Jagota and M. Chaudhury for the use of channel fabrication equipment, Z. Song for particle preparation, and P. Kumnorkaew for help in particle characterization. The mask wafers of microchannels were fabricated at the Cornell NanoScale Facility, a member of the National Nanotechnology Infrastructure Network (NSF Grant No. ECS-0335765). This material is based upon work supported by the National Science Foundation (Grant No. 0630191), and funding from the ACS Petroleum Research Fund and North American Mixing Forum.

[1] J. Ottino, *The Kinematics of Mixing* (Cambridge University Press, Cambridge, England, 1989).
[2] R. Liu, K. Sharp, M. Olsen, M. Stremler, J. Santiago, R. Adrian, H. Aref, and D. Beebe, J. Microelectromech. Syst. **9**, 190 (2000).
[3] V. Mengeaud, J. Josserand, and H. Girault, Anal. Chem. **74**, 4279 (2002).
[4] F. Schönfeld, V. Hessel, and C. Hofmann, Lab Chip **4**, 65 (2004).
[5] V. Hessel, H. Lowe, and F. Schönfeld, Chem. Eng. Sci. **60**, 2479 (2005).
[6] A. Stroock, S. Dertinger, A. Ajdari, I. Mezic, H. Stone, and G. Whitesides, Science **295**, 647 (2002).
[7] D. Leighton and A. Acrivos, J. Fluid Mech. **181**, 415 (1987).
[8] C. Gao and J. F. Gilchrist, Phys. Rev. E **77**, 025301(R) (2008)
[9] M. Lopez and M. Graham, Phys. Fluids **20**, 053304 (2008).
[10] D. Lee, J. Paint Technol.. **42**, 579 (1970).
[11] A. P. Shapiro and R. F. Probstein, Phys. Rev. Lett. **68**, 1422 (1992).
[12] D. He and N. Ekere, Rheol. Acta **40**, 591 (2001).
[13] F. Horn and W. Richtering, J. Rheol. **44**, 1279 (2000).
[14] M. Lyon and L. Leal, J. Fluid Mech. **363**, 57 (1998).
[15] A. Shauly, A. Wachs, and A. Nir, J. Rheol. **42**, 1329 (1998).
[16] D. Semwogerere and E. Weeks, Phys. Fluids **20**, 043306 (2008).
[17] J. Norman, B. Oguntade, and R. Bonnecaze, J. Fluid Mech. **594**, 1 (2008).
[18] Y. Xia and G. Whitesides, Annu. Rev. Mater. Sci. **28**, 153 (1998).
[19] P. Nott and J. Brady, J. Fluid Mech. **275**, 157 (1994).
[20] J. Crocker and D. Grier, J. Colloid Interface Sci. **179**, 298 (1996).
[21] A. Ramachandran and D. Leighton, Phys. Fluids **19**, 053301 (2007).
[22] R. Hampton, A. Mammoli, A. Graham, N. Tetlow, and S. Altobelli, J. Rheol. **41**, 621 (1997).
[23] P. Danckwerts, Appl. Sci. Res., Sect. A **3**, 279 (1952).
[24] M. Lyon and L. Leal, J. Fluid Mech. **363**, 25 (1998).
[25] R. Miller and J. Morris, J. Non-Newtonian Fluid Mech. **135**, 149 (2006).
[26] J. Morris and F. Boulay, J. Rheol. **43**, 1213 (1999).
[27] M. Frank, D. Anderson, E. Weeks, and J. Morris, J. Fluid Mech. **493**, 363 (2003).